Biomechanical Characterization of Keratoconus Corneas Ex Vivo With Brillouin Microscopy

Giuliano Scarcelli,[1,2] Sebastien Besner,[1,2] Roberto Pineda,[3] and Seok Hyun Yun[1,2,4]

[1]Wellman Center for Photomedicine, Massachusetts General Hospital, Cambridge, Massachusetts, United States
[2]Department of Dermatology, Harvard Medical School, Boston, Massachusetts, United States
[3]Department of Ophthalmology, Massachusetts Eye and Ear Infirmary, Boston, Massachusetts, United States
[4]Harvard-MIT Health Sciences and Technology, Cambridge, Massachusetts, United States

Correspondence: Giuliano Scarcelli, 65 Landsdowne Street, Cambridge, MA 02139, USA; scarcelli.giuliano@mgh.harvard.edu. Seok Hyun Yun; syun@hms.harvard.edu.

GS and SB contributed equally to the work presented here and should therefore be regarded as equivalent authors.

Submitted: March 26, 2014
Accepted: June 5, 2014

Citation: Scarcelli G, Besner S, Pineda R, Yun SH. Biomechanical characterization of keratoconus corneas ex vivo with Brillouin microscopy. *Invest Ophthalmol Vis Sci*. 2014;55:4490–4495. DOI:10.1167/iovs.14-14450

Purpose. Loss of corneal strength is a central feature of keratoconus progression. However, it is currently difficult to measure corneal mechanical changes noninvasively. The objective of this study is to evaluate if Brillouin optical microscopy can differentiate the mechanical properties of keratoconic corneas versus healthy corneas ex vivo.

Methods. We obtained eight tissue samples from healthy donor corneas used in Descemet's stripping endothelial keratoplasty (DSEK) and 10 advanced keratoconic corneas from patients undergoing deep anterior lamellar keratoplasty (DALK). Within 2 hours after surgery, a confocal Brillouin microscope using a monochromatic laser at 532 nm was used to map the Brillouin frequency shifts of the corneas.

Results. The mean Brillouin shift in the anterior 200 μm of the keratoconic corneas at the cone was measured to be 7.99 ± 0.10 GHz, significantly lower than 8.17 ± 0.06 GHz of the healthy corneas ($P < 0.001$). The Brillouin shift in the keratoconic corneas decreased with depth from the anterior toward posterior regions with a steeper slope than in the healthy corneas ($P < 0.001$). Within keratoconic corneas, the Brillouin shift in regions away from the apex of the cone was significantly higher than within the cone region ($P < 0.001$).

Conclusions. Brillouin measurements revealed notable differences between healthy and keratoconic corneas. Importantly, Brillouin imaging showed that the mechanical loss is primarily concentrated within the area of the keratoconic cone. Outside the cone, the Brillouin shift was comparable with that of healthy corneas. The results demonstrate the potential of Brillouin microscopy for diagnosis and treatment monitoring of keratoconus.

Keywords: Brillouin microscopy, keratoconus, corneal biomechanics

Keratoconus affects approximately 1 in 2000 people in the general population.[1] Clinically, advanced keratoconus is characterized by thinning and steepening of the cornea. Such dramatic manifestations, however, represent end stage progression of this degenerative disorder. Recent studies at the genetic and molecular level have shed light on the etiology of the disease. In particular, collagen and extracellular matrix pathways were found to be linked to keratoconus.[2] Upregulation of matrix metalloproteinase (MMP)[3] production and decreased lysyl oxidase (LOX) activity,[4] which affects collagen cross-linking, have been reported in patients with keratoconus as well as altered collagen organizations within the corneal stroma.[5,6] All of these findings point to a reduced mechanical stability of the keratoconic cornea. Mechanical measurements of extracted cornea tissues have provided direct evidence of mechanical weakening in advanced keratoconic corneas. Andreassen et al.[7] measured stress–strain curves with corneal strips to show reduced elastic modulus in keratoconic corneas. These results were later confirmed by Nash et al.[8] and Edmund.[9] The loss of biomechanical stability is thought to drive the morphologic changes and, therefore, may be an appropriate target to diagnose the onset and the rate of the progression of the morphologic changes.[10–13]

Current clinical instruments, such as pachymetry and topography, can detect abnormal morphologic patterns in keratoconic corneas, but cannot measure the mechanical stability. There has been increasing interest in developing an instrument to measure the mechanical properties of the cornea for more objective diagnostics of keratoconus and improved screening of patients at-risk for post-LASIK ectasia. The Ocular Response Analyzer,[14] which measures corneal hysteresis, has shown to distinguish advanced keratoconic corneas from healthy ones,[15] but owing to the low sensitivity and specificity of the hysteresis-only based measurement, its clinical value remains to be validated.[16,17] Dynamic imaging in combination with air puff can measure different deformation profiles between healthy and keratoconic corneas,[18–21] but such measurements involving physical deformation of the cornea are inherently coupled with IOP and other geometrical factors[22] (Roberts CJ, et al. *IOVS* 2011;52:ARVO E-Abstract 4384). Second harmonic generation (SHG) microscopy has shown the ability to map corneal collagen organization[23] and recent modeling studies have shown that corneal elastic modulus could be derived from cross-sectional SHG images that quantify collagen structure[24,25]; however, this technique is not yet available for clinical studies.[26]

Copyright 2014 The Association for Research in Vision and Ophthalmology, Inc.

Recently, we have developed Brillouin microscopy[27] for noncontact three-dimensional (3D) mapping of corneal modulus[28] and measurement of corneal stiffening by corneal collagen crosslinking.[29,30] Brillouin microscopy is based on Brillouin scattering that arises from the interaction between light incident on a medium of interest and spontaneous acoustic phonons within the medium. As the propagation speeds of acoustic phonons are related to the material's mechanical properties, measuring the frequency shift induced by the acousto-optic interaction allows the elastic properties to be determined. This technique works with low-power, near-infrared, laser light safe for clinical uses.[31] Here, we report on our ex vivo study to investigate the ability of Brillouin microscopy to differentiate keratoconic corneas from healthy corneas based on Brillouin frequency shifts.

Materials and Methods

Brillouin Microscope

The Brillouin microscope is comprised of a standard inverted confocal microscope and a double Virtually Imaged Phased Array (VIPA) spectrometer (Fig. 1a).[32,33] For ex vivo measurements, we used a single-frequency laser at a wavelength of 532 nm with optical power of 4 mW on the sample. The probe light was focused on the cornea sample (Fig. 1b) by using an objective lens with numerical aperture of 0.25 to yield a lateral resolution approximately 1 μm and axial resolution approximately 8 μm. The cornea sample was placed in a moist chamber mounted on a 3-axis motorized stage (Prior Scientific, Rockland, MA, USA). A wet cloth was placed in the closed-dish chamber to maintain the humidity (Fig. 1c). The scattered light from a cornea sample was collected by a single-mode optical fiber (Thorlabs, Newton, NJ, USA) and coupled into the VIPA spectrometer. The spectrum was recorded with an EM-CCD camera (Ixon Du197; Andor, Belfast, UK) with a frame integration time of 200 ms. The Charged-Coupled Device (CCD) data were processed to determine the Brillouin frequency shifts by using a custom-written MATLAB code (Mathworks, Natick, MA, USA). Brillouin images plot the measured frequency shifts with color encoding.

Brillouin Shift Relationship to Standard Elastic Moduli

The Brillouin frequency shift Ω reported in this paper is related to the real part of longitudinal viscoelastic modulus $M' = \rho\lambda^2\Omega^2/4n^2$, where ρ is the mass density, λ is the optical wavelength and n is the refractive index. The longitudinal modulus can be expressed in terms of Young's modulus E' and the Poisson's ratio σ at a frequency range of 5 to10 GHz: that is, $M' = E'(1-\sigma)/(1+\sigma)(1-2\sigma)$. We have previously shown that the longitudinal modulus M' determined from the Brillouin shift is related to conventional Young's (or shear) moduli E' measured at low frequencies (e.g., 1 Hz) through a log-log linear relationship: $log(M') = alog(E') + b$, where a and b are material-dependent coefficients.[30,34] The relative change can be expressed as:

$$\delta E'/E' = (1/a)\delta M'/M' \quad (1)$$

where the conversion factor, $1/a$, was measured to approximately 30 for porcine corneas (Besner S, et al., *IOVS* 2014;55: ARVO E-Abstract 3718). This conversion factor is consistent with the previously reported comparison of Brillouin data to shear moduli on corneal crosslinking[30] and with the anterior-to-posterior changes measured in this manuscript in healthy corneas compared with previously published data obtained with standard mechanical tests.[23]

Cornea Tissue Samples

Full or partial central corneal buttons (8 mm in diameter; Fig. 1b) were obtained as discarded tissue after surgery. The protocol was approved by the Partners Human Research Committee, and all the procedures conformed to the tenets of the Declaration of Helsinki. For healthy controls, donor corneas in the age range of 33- and 64-years old were obtained from Descemet's stripping endothelial keratoplasty (DSEK) procedure. As part of this procedure, only the posterior cornea (90–120 μm) is needed for the surgery; as a result, the majority of the anterior portion of the cornea was available for our analysis. Keratoconic tissue samples were obtained from patients undergoing deep anterior lamellar keratoplasty (DALK) surgery in the age range of 26- and 51-years old. In this procedure, the Descemet's membrane and endothelium of the keratoconic cornea are maintained, whereas the epithelium and stroma are removed and replaced by donor tissue. Thus, the dissected anterior portion of the cornea was available for our analysis. In terms of tissue extraction, the two procedures do not involve mechanical damage to the tissue under examination. All samples were collected immediately, stored in Optisol solution (Bausch & Lomb, Irvine, CA, USA), and transported to the Brillouin microscope. All the Brillouin measurements were completed within 2 hours after surgery.

Determining Spatial Location on Cornea Tissue Samples

To analyze the regional variation of mechanical properties, the cornea samples were marked by the surgeon with a central ink-dot and with several marks at the radial edge (Fig. 1b). Because the ink strongly absorbs the green laser light, Brillouin measurements were performed in locations away from the ink marks. In healthy corneas, several randomly selected regions 1 to 4 mm away from the center of the sample were measured. For keratoconic corneas, the position of the cone determined by the surgeon based on pre-operative maps were indicated by using the ink marks as reference. Measurements were made over a 2×2–mm area in the cone region. In four keratoconus samples, we were able to take Brillouin measurements in a peripheral region (2×2 mm) in the opposite side of the keratoconus cone, at least 4 mm away from the cone center.

Results

Depth-Dependent Mechanical Properties of Healthy Versus Keratoconic Corneas

The cross-sectional Brillouin image (x-z plane) of healthy human corneal tissue (Fig. 2a) reveals the depth-dependent variation of Brillouin shift, consistent with previous in vivo data from a healthy volunteer.[31] In contrast, the cross-sectional image of the cone region in a keratoconic cornea (Fig. 2b) shows dramatic differences from the healthy state. The keratoconus sample displays overall much smaller Brillouin shifts and more rapid decrease of the Brillouin shifts through depth.

Figures 3a and 3b show representative depth profiles of Brillouin measurements for several healthy corneas and keratoconic corneas in the cone region. The axial profiles of healthy corneas present high Brillouin shifts in the anterior portion of the stroma. The depth dependence is clearly divided

Investigative Ophthalmology & Visual Science

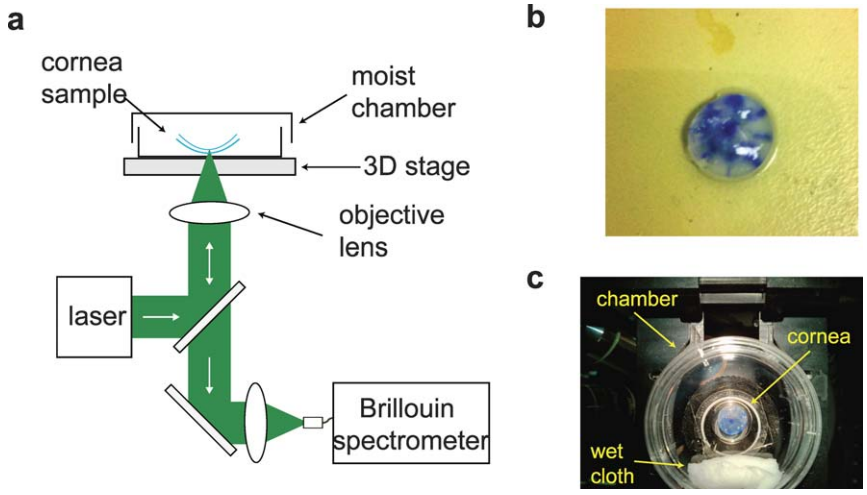

Figure 1. Experimental Setup. (**a**) Schematic of the measurement setup. (**b**) Representative picture of a typical corneal central "button" sample. The *blue ink marks* helped identify the position of the cone (see also insets in Fig. 3). (**c**) The sample is placed face down on a glass-bottom culture dish with a wet cloth to keep the moist environment during measurements.

into two regions: the anterior region of moderate decay and the posterior region of steep decline over depth. The profiles of keratoconic corneas measured in the cone region, as shown in Figure 3b, are dramatically different from the healthy ones. The anterior portion of the cornea has low Brillouin shift, and the shift monotonically decays in a rapid fashion across depth. In addition, the keratoconus cone profiles present much higher cornea-to-cornea variability in terms of Brillouin shift and changes through depth compared with healthy controls.

Regional Variations Within Healthy and Keratoconic Corneas

Beyond the cornea-to-cornea comparisons, we used the high resolution of Brillouin microscopy to investigate the regional variations within our cornea samples. Within healthy corneas, we found small variations in Brillouin shift as a function of spatial location of the depth profile, close to the measurement uncertainty, hinting that the central region of healthy corneas has fairly uniform mechanical modulus. In contrast, keratoconic corneas showed much higher regional variations. To analyze this feature, within keratoconic corneas, we took two series of measurements, in the vicinity of the cone region (Fig. 3b) and at least 4-mm outside the cone region (Fig. 3c). The profiles shown in Figure 3c, measured in the regions outside the cone, were all distinctly different from those of the cone regions in Figure 3b, and rather similar to those of healthy corneas in Figure 3a.

Brillouin Metrics to Characterize Keratoconic Corneas

Figure 4a shows the anterior Brillouin shift of healthy ($N = 8$), keratoconus in the cone region ($N = 10$), and keratoconus outside the cone region ($N = 4$) computed as the average Brillouin shift in the anterior 200-μm region of each depth profile. A highly statistically significant decrease (unpaired *t*-test, $P < 0.001$) is shown in the keratoconic cone region (7.99 ± 0.10 GHz) with respect to the healthy controls (8.17 ± 0.06 GHz). Also, a highly statistically significant difference (unpaired *t*-test, $P < 0.001$) is shown between the cone and noncone regions (8.19 ± 0.04 GHz). On the other hand, the noncone regions show no statistically significant difference compared with healthy corneas. In Figure 4b we compare the slope, or rate of decrease through depth (computed across the anterior 350–400–μm depth). The cone regions present a much steeper decline (unpaired *t*-test, $P < 0.001$) in Brillouin shift (–0.93 ± 0.29 GHz/mm) with respect to the healthy controls (–0.38 ± 0.17 GHz/mm). Similarly, the cone regions present a much steeper decline in Brillouin shift (unpaired *t*-test, $P < 0.001$) compared with regions away from the cone (–0.53 ± 0.15 GHz/mm). On the other hand, the noncone regions show no statistically significant difference in depth-dependence of Brillouin shift compared with healthy corneas. In both these metrics, namely anterior mean Brillouin shift and axial slope,

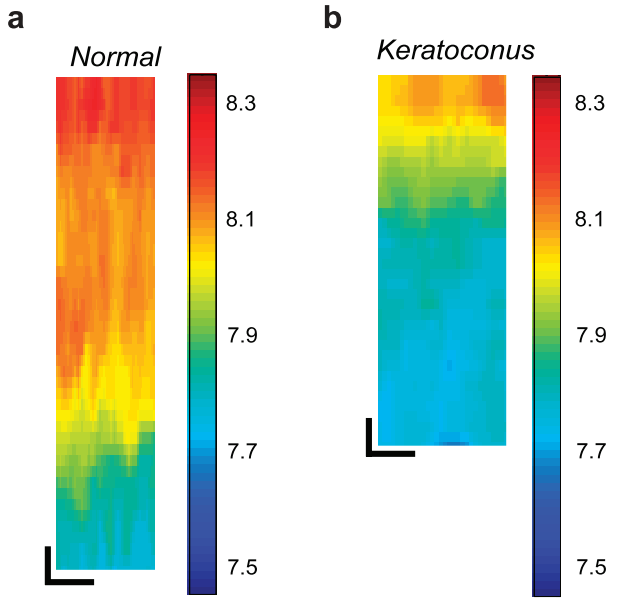

Figure 2. Representative cross-sectional (*x-z*) Brillouin images of human cornea tissue samples. (**a**) Anterior portion of a healthy cornea from a nonkeratoconus donor collected after DSEK surgery. (**b**) Anterior portion of a keratoconus cornea collected after DALK surgery imaged within the cone region. *Scale bars*: 50 μm.

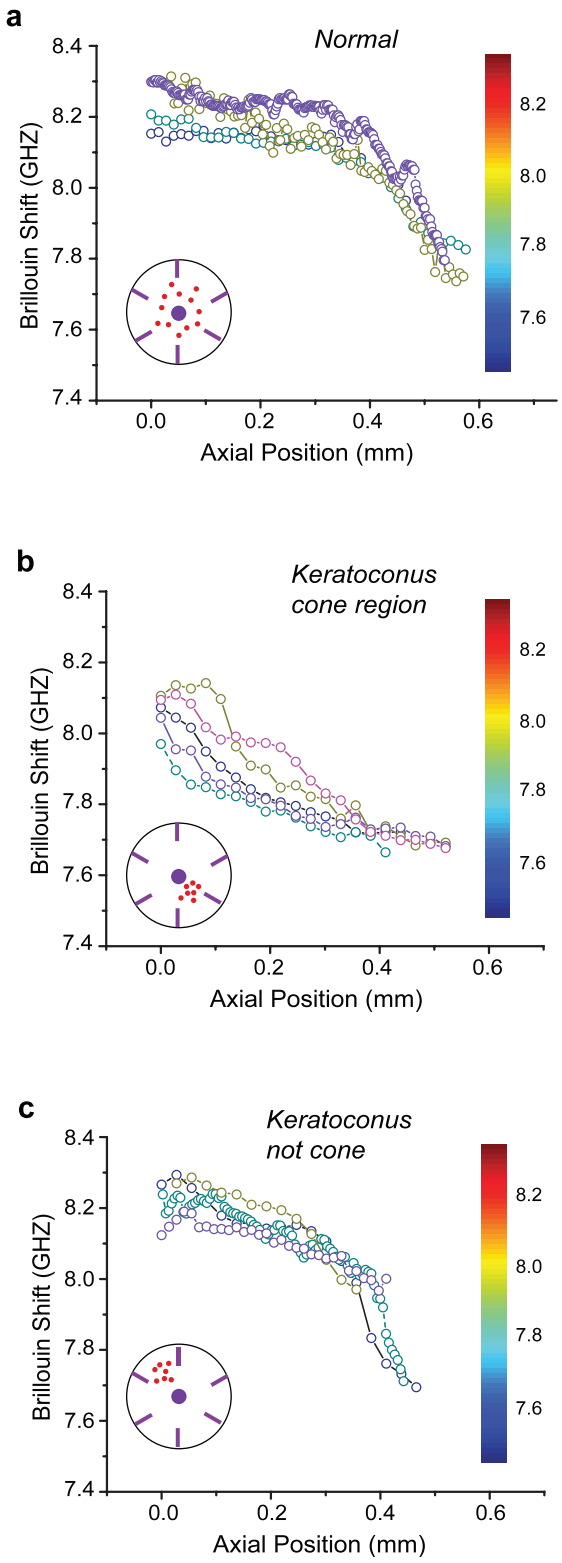

Figure 3. Brillouin depth profiles of several cornea tissue samples. Each colored profile indicates a representative depth profile from a different cornea. The depth profile was typically obtained by an average of 10 to 20 axial scans at a given location. The *red dots* in the inset indicate the regions of all the measurements ($N = 10$ from four different corneas). (**a**) Along the depth axis, healthy corneas are characterized by slightly decreasing anterior modulus followed by a more rapid decline in the midposterior stroma. (**b**) In the cone region of keratoconus corneas, the Brillouin depth profile show lower Brillouin modulus and more rapid decline of modulus across depth. (**c**) Outside the cone region, keratoconus corneas present similar Brillouin depth profiles as healthy corneas.

the cone regions present higher variability between samples compared to both healthy controls and outside-cone regions in keratoconic corneas.

Discussion

In this study, we performed high-resolution noncontact mechanical characterization of human cornea tissue samples collected from keratoconic corneas and healthy controls. Overall, the Brillouin measurements indicated that keratoconic corneas have substantially lower Brillouin shifts than healthy corneas. This result implies that keratoconic corneas present lower elastic modulus than healthy controls. The log–log relationship (see Materials and Methods) allows us to estimate the magnitude of change of shear or Young's moduli in the keratoconic corneas.[30] From our Brillouin results, the relative decrease of these conventional moduli in the cone compared with the healthy corneas is approximately a factor of two, while the periphery of keratoconic corneas has similar modulus to healthy corneas. This significant decrease is consistent with the 70% reduction in Young's modulus previously found by Andreassen et al.[7] with tensile tests on corneal strips.

As in other ex vivo studies, one of the limitations of our measurement is the possible influence of the hydration/swelling of samples. Although all our experiments were conducted within 2 hours from surgery, some degree of swelling is not avoidable, especially because our cornea samples did not have endothelium. Hydration and swelling affect the actual mechanical properties of the cornea samples and may introduce an artifact in Brillouin measurement readings. Keratoconic corneas have been reported to be more prone to swelling than healthy corneas (Muller LJ, et al. *IOVS* 2004;45:ARVO E-Abstract 3824). However, based on the observed similarity in the Brillouin profiles between the healthy and the noncone keratoconus cornea, it is unlikely that post operational swelling caused a major artifact. In addition, Muller et al.[35] have shown that in both normal and keratoconic corneas swelling is mostly limited to the posterior portion of the cornea while the collagen fiber network prevents significant swelling in the anterior stroma (Muller LJ, et al. *IOVS* 2004;45:ARVO E-Abstract 3824). Therefore, we expect that the anterior Brillouin shifts measured in our study are likely to recapitulate the in vivo behavior. However, our measurement of the rate of change across depth, or axial slope, might be exaggerated due to the differential swelling of anterior and posterior cornea. To infer the elastic modulus from the Brillouin shift measurement the value of ρ/n^2 is required. The refractive index and density are not spatially uniform and depend on the hydration state of the cornea. Therefore, swelling may cause an artifact in the measurement. The human corneas in the normohydrated conditions (~3.5 $mg_{H2O}/mg_{drytissue}$) have been reported to have refractive index of 1.376 and density of 1.07 g/mL, while corneas in highly swollen conditions (~7.5 $mg_{H2O}/mg_{drytissue}$) have been reported to have refractive index of 1.362 and density of 1.04 g/ml.[36,37] In our experimental conditions, we estimated the variation in hydrations not to exceed approximately 5 $mg_{H2O}/mg_{drytissue}$. Hence, the range of variation for ρ/n^2 is estimated between 0.565 g/mL and 0.5635 g/ml. In these conditions, the conversion of Brillouin shifts in longitudinal

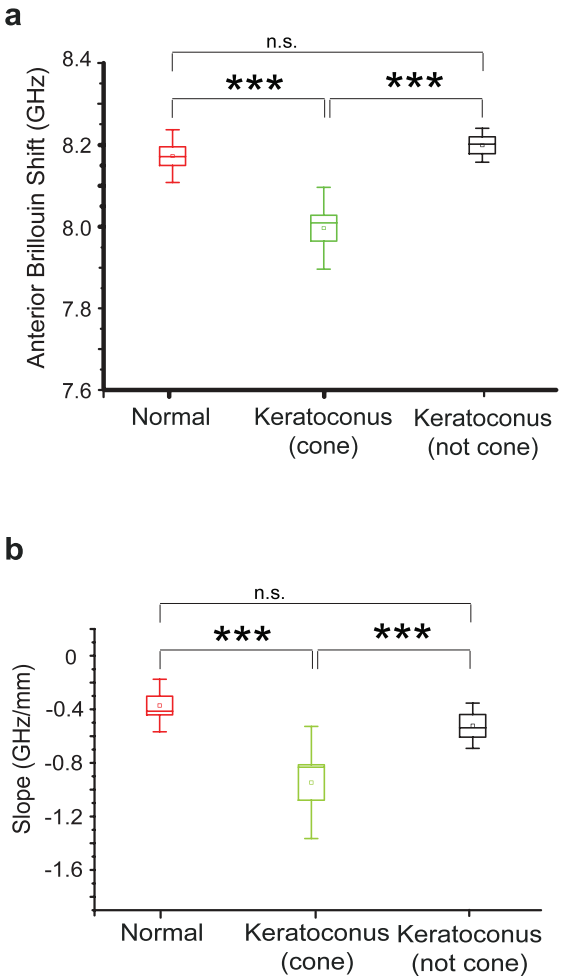

Figure 4. Brillouin elasticity metrics. (**a**) The Brillouin shift in the anterior 200 μm of keratoconic corneas measured within the cone region is significantly lower than in healthy corneas and in regions of keratoconic corneas outside the cone. Regions away from the cone do not display significant differences from healthy corneas. (**b**) The axial slope, or rate of change in Brillouin shift through depth, within the cone region is significantly steeper than the one measured in healthy corneas and in keratoconus corneas outside the cone. The noncone regions do not display significant differences from healthy corneas. ***$P < 0.001$; n.s., not statistically significant difference.

moduli is expected to be affected by less than approximately 0.3%.

In general, age can be a confounding factor for corneal biomechanical measurements.[38] In our study, healthy control corneas were taken from donors of 52 ± 13 years of age, while keratoconic corneas were taken from patients of 41 ± 10 years of age. A small increase of Brillouin shift with age was observed among the normal donor corneas. However, the increase was not statistically significant ($R \sim 0.36$) and may be affected by variability in the sample preparation. The Brillouin shift and slope of healthy versus keratoconus corneas showed high statistically significant differences also accounting for age with a multiple regression model ($P < 0.005$). In addition, the Brillouin shifts measured in the keratoconic corneas away from the cone show similar values with the healthy control group. Therefore, we conclude that the contribution of age dependence was minor, if not negligible, in this study.

Importantly, we identified significant heterogeneity in the spatial distribution of Brillouin shift within keratoconic corneas. Low Brillouin shifts were measured only within the cone region. The outside-cone regions in the keratoconic corneas were similar to the healthy corneas in terms of Brillouin shifts. These results may be related with electron microscopy studies by Radner et al.[39] and x-ray studies by Meek et al.,[5] which showed that within keratoconic corneas the apical regions featured altered collagen organization with respect to normal while other regions did not differ significantly from healthy corneas. Also, recent experiments using second harmonic generation on keratoconic corneas noted a decrease in collagen fiber branching and fiber insertion to Bowman's layer limited to the cone area of keratoconic corneas, which suggests an overall weakening of the stroma in the area of the cone (J. Jester, personal written communication, 2014).

It has been proposed that the asymmetric spatial distribution of corneal biomechanical properties within the cornea is a crucial, early event in the progression of keratoconus.[40] This hypothesis was tested with topographic analysis on an experimental model of keratoconus based on collagenase-induced softening and computer simulations.[41] Our study provides experimental data that spatial asymmetry in the distribution of elastic modulus indeed exists in keratoconic corneas, whereas it is not present in healthy corneas. In this scenario, the potential of using a criterion based on the spatial variation of Brillouin shifts seems promising. This type of metric may be particularly suited to detect the early onset and progression of keratoconus.

In conclusion, this study has demonstrated that Brillouin microscopy is a sensitive tool to detect the mechanical differences between healthy and keratoconic corneas with high spatial resolution. Two distinctive features, the anterior Brillouin shift and axial slope, were found to be significantly different between healthy and keratoconic corneas and between keratoconic cone and noncone regions. These results demonstrate the significant potential of Brillouin-based measurements for clinical characterization of keratoconus patients toward early diagnosis for keratoconus and screening for keratorefractive surgery.

Acknowledgments

The authors thank Cynthia J. Roberts for helpful discussions.

Supported by grants from Harvard Clinical and Translational Science Center (National Institutes of Health UL1-RR025758; Bethesda, MD, USA), American Society for Laser Medicine and Surgery (Wasau, WI, USA), National Institutes of Health (P41-EB015903, R21EY023043, K25EB015885; Bethesda, MD, USA), National Science of Foundation (CBET-0853773; Washington, DC, USA), and Human Frontier Science Program (Strasbourg, France).

Disclosure: **G. Scarcelli**, P; **S. Besner**, None; **R. Pineda**, Amgen (C), Angiotech (C); **S.H. Yun**, P

References

1. Krachmer JH, Feder RS, Belin MW. Keratoconus and related noninflammatory corneal thinning disorders. *Surv Ophthalmol*. 1984;28:293–322.
2. Lu Y, Vitart V, Burdon KP, et al. Genome-wide association analyses identify multiple loci associated with central corneal thickness and keratoconus. *Nat Genet*. 2013;45:155–163.
3. Seppälä HP, Määttä M, Rautia M, et al. EMMPRIN and MMP-1 in keratoconus. *Cornea*. 2006;25:325–330.
4. Dudakova L, Liskova P, Trojek T, Palos M, Kalasova S, Jirsova K. Changes in lysyl oxidase (LOX) distribution and its decreased activity in keratoconus corneas. *Exp Eye Res*. 2012;104:74–81.
5. Meek KM, Tuft SJ, Huang Y, et al. Changes in collagen orientation and distribution in keratoconus corneas. *Invest Ophthalmol Vis Sci*. 2005;46:1948–1956.

6. Morishige N, Wahlert AJ, Kenney MC, et al. Second-harmonic imaging microscopy of normal human and keratoconus cornea. *Invest Ophthalmol Vis Sci*. 2007;48:1087–1181.
7. Andreassen TT, Simonsen AH, Oxlund H. Biomechanical properties of keratoconus and normal corneas. *Exp Eye Res*. 1980;31:435–441.
8. Nash IS, Greene PR, Foster CS. Comparison of mechanical properties of keratoconus and normal corneas. *Exp Eye Res*. 1982;35:413–424.
9. Edmund C. Corneal elasticity and ocular rigidity in normal and keratoconis eyes. *Acta Ophthalmol*. 1988;66:134–140.
10. Maguire LJ, Bourne WM. Corneal topography of early keratoconus. *Am J Ophthalmol*. 1989;108:107–112.
11. Rabinowitz YS. Videokeratographic indexes to aid in screening for keratoconus. *J Refract Surg*. 1995;11:371–379.
12. Li XH, Rabinowitz YS, Rasheed K, Yang HY. Longitudinal study of the normal eyes in unilateral keratoconus patients. *Ophthalmology*. 2004;111:440–446.
13. Li XH, Yang HY, Rabinowitz YS. Keratoconus: classification scheme based on videokeratography and clinical signs. *J Cataract Refract Surg*. 2009;35:1597–1603.
14. Luce DA. Determining in vivo biomechanical properties of the cornea with an ocular response analyzer. *J Cataract Refract Surg*. 2005;31:156–162.
15. Shah S, Laiquzzaman M, Bhojwani R, Mantry S, Cunliffe I. Assessment of the biomechanical properties of the cornea with the ocular response analyzer in normal and keratoconic eyes. *Invest Ophthalmol Vis Sci*. 2007;48:3026–3031.
16. Fontes BM, Ambrosio R Jr, Velarde GC, Nose W. Ocular response analyzer measurements in keratoconus with normal central corneal thickness compared with matched normal control eyes. *J Refract Surg*. 2011;27:209–215.
17. Fontes BM, Ambrosio R Jr, Jardim D, Velarde GC, Nose W. Corneal biomechanical metrics and anterior segment parameters in mild keratoconus. *Ophthalmology*. 2011;117:673–679.
18. Ambrosio R Jr, Caldas D, Ramos I, Santos R, Belin M. Corneal biomechanical assessment using dynamic ultra high-speed Scheimpflug technology non-contact tonometry (UHS-ST NCT): preliminary results. Presented at: American Society of Cataract and Refractive Surgery-American Society of Ophthalmic Administrators (ASCRS-ASOA) Symposium and Congress. March 25-29, 2011; San Diego, CA.
19. Ford MR, Dupps WJ Jr, Rollins AM, Roy AS, Hu Z. Method for optical coherence elastography of the cornea. *J Biomed Opt*. 2011;16:016005.
20. Grabner G, Eilmsteiner R, Steindl C, Ruckhofer J, Mattioli R, Husinsky W. Dynamic corneal imaging. *J Cataract Refract Surg*. 2005;31:163–174.
21. Tanter M, Touboul D, Gennisson J-L, Bercoff J, Fink M. High-resolution quantitative imaging of cornea elasticity using supersonic shear imaging. *IEEE Trans Med Imaging*. 2009; 28:1881–1893.
22. Dorronsoro C, Pascual D, Perez-Merino P, Kling S, Marcos S. Dynamic OCT measurement of corneal deformation by an air puff in normal and cross-linked corneas. *Biomed Opt Express*. 2012;3:473–487.
23. Winkler M, Chai D, Kriling S, et al. Non-linear optical macroscopic assessment of 3-D corneal collagen organization and axial biomechanics. *Invest Ophthalmol Vis Sci*. 2011;52: 8818–8827.
24. Petsche SJ, Chernyak D, Martiz J, Levenston ME, Pinsky PM. Depth-dependent transverse shear properties of the human corneal stroma. *Invest Ophthalmol Vis Sci*. 2012;53:873–880.
25. Petsche SJ, Pinsky PM. The role of 3-D collagen organization in stromal elasticity: a model based on X-ray diffraction data and second harmonic-generated images. *Biomech Model Mechanobiol*. 2014;12:1101–1113.
26. Latour G, Gusachenko I, Kowalczuk L, Lamarre I, Schanne-Klein M-C In vivo structural imaging of the cornea by polarization-resolved second harmonic microscopy. *Biomed Opt Express*. 2012;3:1–15.
27. Scarcelli G, Yun SH. Brillouin confocal microscopy for three-dimensional mechanical imaging. *Nat Photonics*. 2008;2:39–43.
28. Scarcelli G, Pineda R, Yun S. Brillouin optical microscopy for corneal biomechanics. *Invest Ophthalmol Vis Sci*. 2012;53: 185.
29. Cherfan D, Verter EE, Melki S, et al. Collagen cross-linking using rose bengal and green light to increase corneal stiffness. *Invest Ophthalmol Vis Sci*. 2013;54:3426–3433.
30. Scarcelli G, Kling S, Quijano E, Pineda R, Marcos S, Yun SH. Brillouin microscopy of collagen crosslinking: noncontact depth-dependent analysis of corneal elastic modulus. *Invest Ophthalmol Vis Sci*. 2013;54:1418–1425.
31. Scarcelli G, Yun SH. In vivo Brillouin optical microscopy of the human eye. *Opt Express*. 2012;20:9197.
32. Scarcelli G, Kim P, Yun SH. Cross-axis cascading of spectral dispersion. *Opt Lett*. 2008;33:2979–2981.
33. Scarcelli G, Yun SH. Multistage VIPA etalons for high-extinction parallel Brillouin spectroscopy. *Opt Express*. 2011;19:10913–10922.
34. Scarcelli G, Kim P, Yun, SH. In vivo measurement of age-related stiffening in the crystalline lens by Brillouin optical microscopy. *Biophys J*. 2011;101:1539–1545.
35. Muller LJ, Pels E, Vrensen G. The specific architecture of the anterior stroma accounts for maintenance of corneal curvature. *Br J Ophthalmol*. 2001;85:437–443.
36. Meek KM, Leonard DW, Connon CJ, Dennis S, Khan S. Transparency, swelling and scarring in the corneal stroma. *Eye*. 2003;17:927–936.
37. Patel S, Alio JL, Perez-Santonja JJ. Refractive index change in bovine and human corneal stroma before and after LASIK: a study of untreated and re-treated corneas implicating stromal hydration. *Invest Ophthalmol Vis Sci*. 2004;45:3523–3530.
38. Elsheikh A, Geraghty B, Rama P, Campanelli M, Meek K. Characterization of age-related variation in corneal biomechanical properties. *R Soc Interface*. 2010;7:1475–1560.
39. Radner W, Zehetmayer M, Skorpik C, Mallinger R. Altered organization of collagen in the apex of keratoconus corneas. *Ophthalmic Res*. 1998;30:327–332.
40. Roberts CJ, Dupps WJ Jr. Biomechanics of corneal ectasia and biomechanical treatments. *J Cataract Refract Surg*. 2014;40: 991–998.
41. Hong CW, Sinha-Roy A, Schoenfield L, McMahon JT, Dupps WJ Jr. Collagenase-mediated tissue modeling of corneal ectasia and collagen cross-linking treatments. *Invest Ophthalmol Vis Sci*. 2014;53:2321–2327.

Investigative Ophthalmology & Visual Science